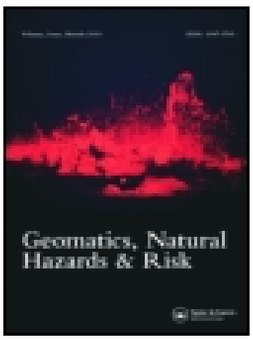

Geomatics, Natural Hazards and Risk

ISSN: 1947-5705 (Print) 1947-5713 (Online) Journal homepage: http://www.tandfonline.com/loi/tgnh20

Modelling desertification risk in the north-west of Jordan using geospatial and remote sensing techniques

Jawad T. Al-Bakri, Laura Brown, Ze'ev Gedalof, Aaron Berg, William Nickling, Saeb Khresat, Mohammad Salahat & Hani Saoub

To cite this article: Jawad T. Al-Bakri, Laura Brown, Ze'ev Gedalof, Aaron Berg, William Nickling, Saeb Khresat, Mohammad Salahat & Hani Saoub (2014): Modelling desertification risk in the north-west of Jordan using geospatial and remote sensing techniques, Geomatics, Natural Hazards and Risk, DOI: 10.1080/19475705.2014.945102

To link to this article: http://dx.doi.org/10.1080/19475705.2014.945102

Geomatics, Natural Hazards and Risk, 2014
http://dx.doi.org/10.1080/19475705.2014.945102

Modelling desertification risk in the north-west of Jordan using geospatial and remote sensing techniques

JAWAD T. AL-BAKRI*†, LAURA BROWN‡, ZE'EV GEDALOF‡, AARON BERG‡, WILLIAM NICKLING‡, SAEB KHRESAT§, MOHAMMAD SALAHAT¶ and HANI SAOUB|

†Department of Land, Water and Environment, Faculty of Agriculture, The University of Jordan, Amman 11942, Jordan
‡Department of Geography, University of Guelph, Guelph, ON, N1G 2W1, Canada
§Department of Natural Resources and the Environment, Jordan University of Science and Technology, Irbid 22110, Jordan
¶Department of Natural Resources and Environment, Hashemite University, Zarqa 13115, Jordan
|Department of Horticulture and Crop Science, Faculty of Agriculture, The University of Jordan, Amman 11942, Jordan

(*Received 8 March 2014; accepted 12 July 2014*)

Remote sensing, climate, and ground data were used within a geographic information system (GIS) to map desertification risk in the north-west of Jordan. The approach was based on modelling wind and water erosion and incorporating the results with a map representing the severity of drought. Water erosion was modelled by the universal soil loss equation, while wind erosion was modelled by a dust emission model. The extent of drought was mapped using the evapotranspiration water stress index (EWSI) which incorporated actual and potential evapotranspiration. Output maps were assessed within GIS in terms of spatial patterns and the degree of correlation with soil surficial properties. Results showed that both topography and soil explained 75% of the variation in water erosion, while soil explained 25% of the variation in wind erosion, which was mainly controlled by natural factors of topography and wind. Analysis of the EWSI map showed that drought risk was dominating most of the rainfed areas. The combined effects of soil erosion and drought were reflected on the desertification risk map. The adoption of these geospatial and remote sensing techniques is, therefore, recommended to map desertification risk in Jordan and in similar arid environments.

1. Introduction

Desertification has become one of the most challenging environmental problems that threaten agricultural production and ecosystem services in arid and semiarid lands. Despite controversy regarding the causes of this problem, the term is most commonly used to indicate irreversible land degradation processes in arid, semiarid, and dry sub-humid areas resulting from various natural and human-induced factors (UNEP 1992; UNCCD 1994).

*Corresponding author. Email: jbakri@ju.edu.jo

Mapping of desertification may include quantification of the status, rate, inherent risk, and/or hazard of the processes contributing to the problem (FAO/UNEP 1984). For planners and decision-makers, spatial information on the risk of desertification is critical to formulate plans and to prioritize proactive actions to sustain and conserve productive lands under the threat of degradation. Traditional methods for mapping desertification risk include the analysis of instrumental climate data and indices (e.g. Al-Hadidi 1996; Millán et al. 2005; Zhai & Feng 2009) to assess changes in rainfall pattern and drought occurrence. As climate does not represent the only factor driving land degradation processes, more complex models for mapping desertification are often required. These models include geospatial and remote sensing techniques to map the extent of degradation as related to soil and vegetation conditions (e.g. Al-Bakri & Taylor 2003; Santini et al. 2010; Saïdi & Gintzburger 2013).

The most important land degradation processes leading to desertification are soil erosion and droughts (UNCCD 2009). Soil erosion becomes problematic in areas with sparse vegetation cover and weak soil structure, where the rate of soil loss exceeds the rate of soil formation or deposition. Natural factors of land topography, rainfall patterns, and wind will also contribute to erosion and will degrade soil structure and fertility, ultimately leading to desertification (Dregne 2002; He et al. 2011). Drought, an extended period of deficiency in water supply resulting from insufficient precipitation in comparison to evapotranspiration, can have substantial impacts on the ecosystem services and agricultural production in the affected regions. Using geospatial and remote sensing techniques to map the extents of soil erosion and drought, therefore, will provide important outputs that describe the spatio-temporal extent of desertification. In addition to time and cost savings, the strength of these techniques is their contribution to the larger spatial domain that can be analysed in terms of desertification patterns and their contributing factors, ultimately informing decisions related to risk management.

Adoption of geospatial and remote sensing techniques to map desertification has been undertaken by many Mediterranean countries, as the potential for desertification to threaten food security in the region is pervasive (Kepner et al. 2006). In Jordan, the national strategy and action plan to combat desertification identifies desertification mapping as a high priority programme, as most of the country's lands are under the threat of desertification (MoEnv 2006). Mapping desertification risk in Jordan, however, requires the adoption of efficient methods and techniques that consider large geographical extents, varying land uses, and biophysical complexity at a reasonable cost and duration. The purpose of this study is to develop an approach to map desertification risk in the north-west of Jordan by combining results from soil erosion and drought models that can be scaled up from regional to national levels, and that can ultimately be implemented in an applied context by land management agencies. The study incorporates results from models of soil erosion by water and wind with those related to drought assessment to generate maps of desertification risk. The maps are statistically assessed in relation to the contributing factors of the land degradation in the study area.

2. Study area and methods

2.1. Study area

The study was carried out in an arid to semiarid area inside the Yarmouk River Basin in Jordan (figure 1). The total area of the basin included in this study was

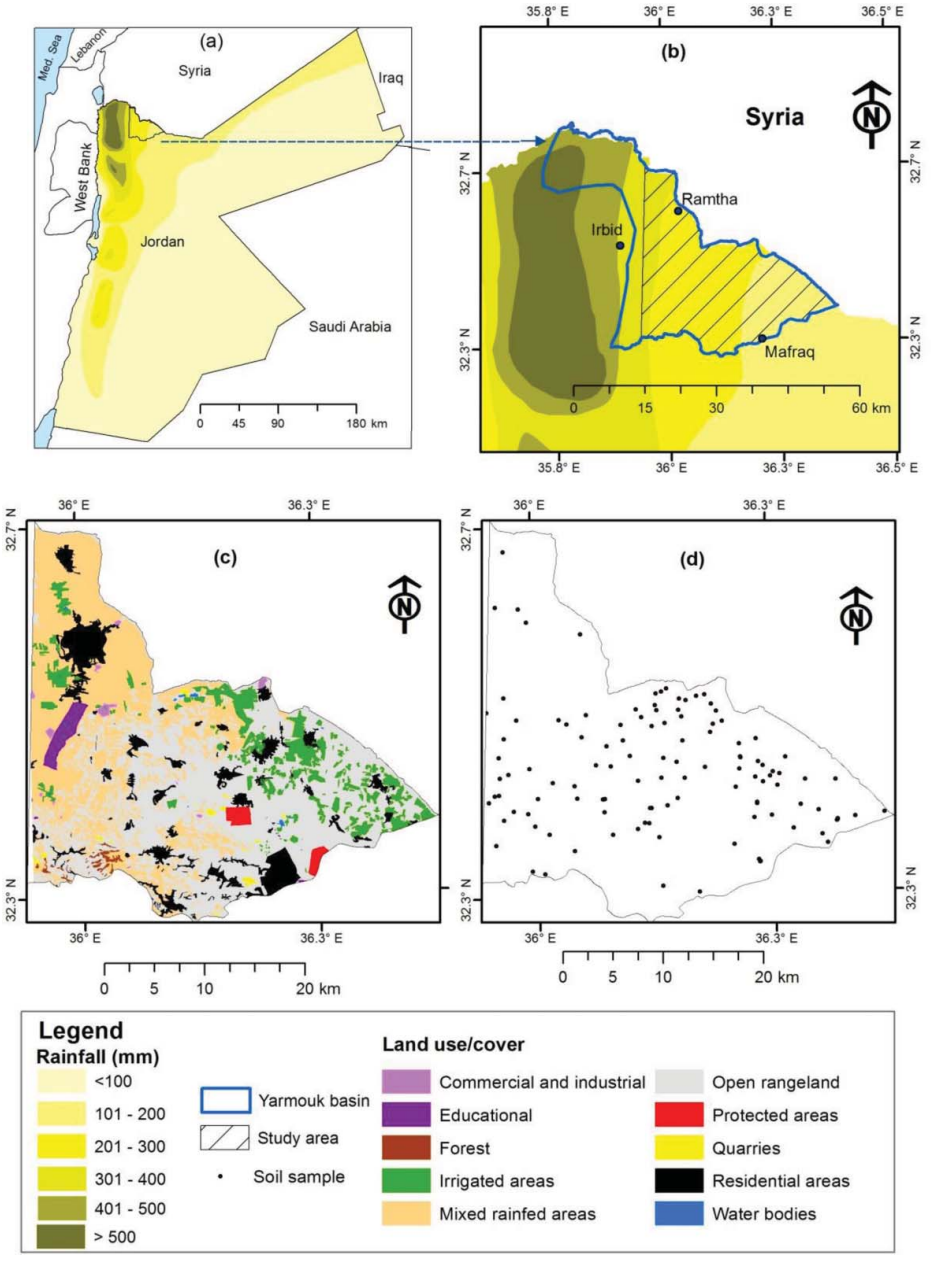

Figure 1. Maps of rainfall distribution in Jordan (a), location of the study area (b), its use/land cover (c), and location of soil sampling sites (d).

989 km^2. The climate of this Mediterranean area is characterized by cool rainy winters and hot dry summers. The annual rainfall of the selected study area varies between 400 mm in the north-west to less than 150 mm in the east. The rainy season typically starts in November and ends by early May. The mean annual potential evaporation ranges between 1500 mm in the west to 2160 mm in the east. The average

temperature range is 22–31 °C in summer and 8–15 °C in winter. The prevailing wind direction is mainly north-westerly in summer and becomes south-westerly in winter, with a speed range of 0.4–25.0 ms^{-1}.

Clayey soils with low carbonate content dominate the western parts of the study area, while aridic soils with high contents of carbonates and silt fraction are found in the east (MoA 1994). Agricultural production in the western parts depends on the rainfed areas of wheat, olives, and vegetables while in the eastern parts, where rainfall is low, it includes the use of rangelands for seasonal browsing. Irrigation is also practiced in the study area, with ground water as the main water source (figure 1).

The main cause of land degradation in the study area is the overgrazing of natural vegetation and crop residues which makes soil susceptible to erosion. The study area is subjected to continuous wind events during early April (spring). These wind events, known as the Khamaseen, cause soil erosion which continues during summer and autumn till the end of November or until the rainy season starts. The area suffers from frequent droughts during late winter and early spring, which affects production of rainfed crops in the dry seasons.

2.2. *Modelling the risk of soil erosion by water*

The universal soil loss equation (USLE) was used to model the risk of soil erosion by water. The USLE combines five different factors to estimate annual soil loss as follows (Wischmeier & Smith 1978; Fistikogli & Harmancioglu 2002):

$$A = R \times K \times L \times S \times C \times P, \tag{1}$$

where A represents the amount of soil loss expressed in ton ha^{-1} $year^{-1}$, R is the rainfall erosivity factor (MJ mm ha^{-1} h^{-1} $year^{-1}$), K is the soil erodibility factor (ton ha h/ha MJ mm), L and S are the slope length and steepness factors (ratios), C is the crop management factor (ratio), and P is the conservation practice factor (ratio).

A spatiao-temporal assessment of soil erosion derived from the USLE model was developed using a geographic information system (GIS) (Khosrokhania & Pradhan 2013). A spatial resolution of 1.0 km was adopted for all coverages for consistency with the MODIS data used in the wind erosion model, and to match the drought data.

The rainfall erosivity factor (R) was prepared in raster format using the Theissen polygon interpolation method of annual rainfall records for the period 1990–2010, for the weather stations of Irbid, Ramtha, and Mafraq. The equation of El-Taif et al. (2010) was used to calculate the values of R from total annual rainfall amounts (f) in the study area as follows:

$$R = 29.12 \times e^{0.0049f}. \tag{2}$$

The soil erodibility factor (K) was computed using the equation of Wischmeier and Smith (1978) as follows:

$$K = (27.66 \times m^{1.14} \times 10^{-8} \times (12 - a)) + (0.0043 \times (b - 2)) + (0.0033 \times (c - 3)), \tag{3}$$

where m is the sum of soil surface contents (%) of sand, silt, and clay, a is the soil surface organic matter (%), b is the soil structure code, and c is the soil profile permeability code. The values of m and a were obtained from digital maps of soil properties created in GIS. The data were obtained for soil samples (figure 1) collected by ground surveys during 2009–2010. The structure and permeability codes were obtained from available soil maps of the study area (MoA 1994).

The slope length (L) and slope steepness (S) factors were computed from a digital elevation model (DEM), derived from the data of the backward channel of the Advanced Spaceborne Thermal Emission and Reflection Radiometer (ASTER). The equation described by Mitasova et al. (1996) was used for the computation of the LS factor at a point $r = (x,y)$ on a hill slope as follows:

$$\mathrm{LS}(r) = (m+1)[A(r)/a_0]^m[\sin b(r)/b_0]^n, \tag{4}$$

where $A(r)$ is an upslope contributing area per unit contour width, $b(r)$ is the slope in degrees, m and n are parameters with values of 0.6 and 1.3; respectively, a_0 is the length (22.1 m or 72.6 ft), and b_0 is the slope.

In order to derive the crop management factor (C), a map of land use/land cover (LULC) was prepared for the study area. The map was based on the visual interpretation of medium resolution (15 m) satellite images of ASTER. The map (figure 1) was verified by ground surveys. Analysis of the map showed that the dominant LULC was open rangelands (45%), followed by rainfed agricultural fields (35%), urban areas (12%), and irrigated farms (8%). The LULC map was used in the model after being resampled to a 1.0-km resolution. The values of C were assigned to each LULC based on previous studies in Jordan (Essa 2004; Al-Zitawi 2006). Modifications for C values were made for rainfed areas and open rangelands according to vegetation cover. This modification was carried out using a relationship developed between the normalized difference vegetation index (NDVI) and vegetation cover in the study area (Al-Bakri et al. 2012). Since no specific management practices (contouring and stripping) were implemented by farmers in the study area, the values of P were based on the slope length map for vegetated and non-vegetated areas and were in the range of 0.5–0.6. Following this stage of map preparation for the USLE factors, all generated layers were multiplied within GIS to produce the map of soil erosion by water (figure 2).

2.3. *Modelling the risk of soil erosion by wind*

Soil erosion by wind was mapped using a wind erosion and dust emission model (WE_DUST_EM), which is GIS-based with a linking code programmed in FORTRAN. The model uses relatively few parameters to characterize the surface and key processes. The factors and processes included in the model are the weather data, soil attributes, surface features, and LULC. Among the weather data, wind speed is the primary factor in initiating wind erosion. Therefore, the model uses the concept of wind threshold shear velocity (u_{*t}) which is the minimum wind force needed to initiate soil particle movement.

Inputs to the model include surface soil properties and characteristics (rock and vegetation cover) and wind field data. They are used to evaluate whether soil erosion by wind will occur within each grid cell that is analysed (figure 3). Soil erosion by wind occurs when the wind shear velocity (u_*) exceeds a soil texture dependent

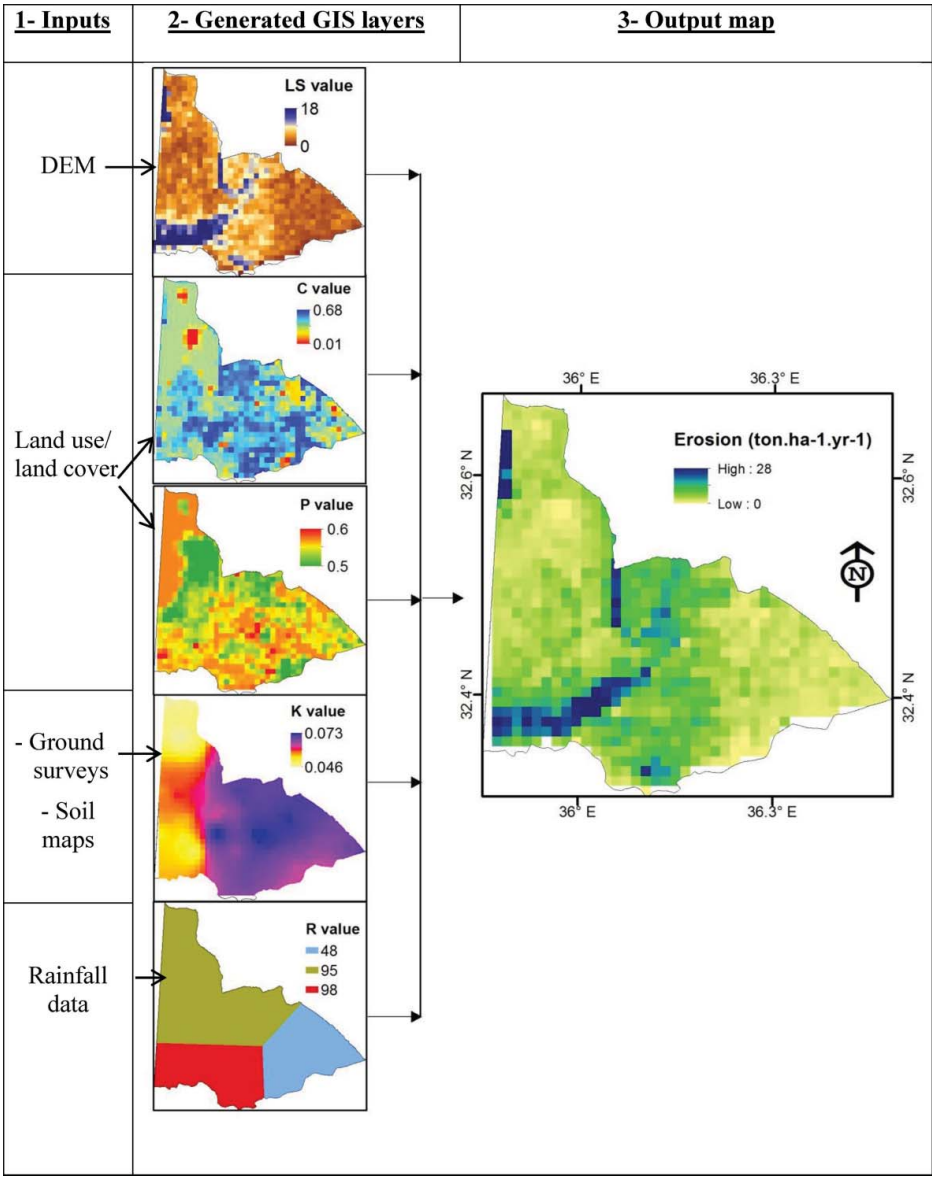

Figure 2. List of input data and GIS layers generated to produce the map of soil erosion by water.

threshold value modified by the presence of surface roughness elements ($u_{*\mathrm{ts}}$). If the condition is satisfied, then soil will erode and the model will calculate the horizontal flux (q) for sand as follows (Namikas & Sherman 1997):

$$q = 2.61\left(\frac{\rho}{g}\right)u_*^3\left(1-\frac{u_{*\mathrm{ts}}}{u_*}\right)\left(1+\left(\frac{u_{*\mathrm{ts}}}{u_*}\right)\right)^2, \tag{5}$$

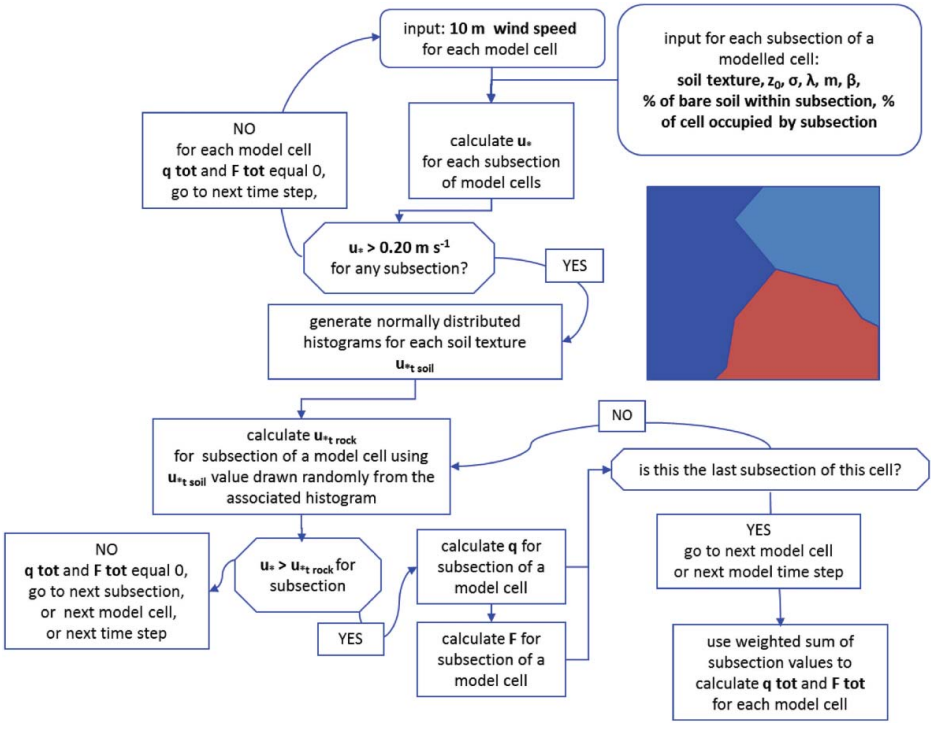

Figure 3. Flowchart of the WE_ DUST_EM model with an example of a model cell divided into three subsections.

where ρ is the air density, g is the gravitational acceleration, u_* is the shear velocity, and $u_{*\mathrm{ts}}$ is the threshold shear velocity associated with a surface soil texture and modified for surface roughness. If u_* for any grid cell does not exceed the threshold ($u_{*\mathrm{ts}}$), this means no soil erosion will occur, and the output value for this grid cell will be zero. If the condition $u_* > u_{*\mathrm{ts}}$ is satisfied, then the horizontal flux is calculated, followed by the calculation of vertical flux (F). In this study, the former was used for assessing the rate of soil erosion by wind, as it was considered representative of sand transport rate in the units of kg m^{-1} s^{-1}. Although there are many sediment discharge models for predicting the rate of soil erosion by wind, the WE_DUST_EM was selected as it provides the best fit to field measurements, especially at shear velocities in excess of 0.2 m s^{-1} (Sarre 1988). The value of $u_{*\mathrm{ts}}$ is calculated as follows (Raupach et al. 1993):

$$u_{*\mathrm{tr}} = u_{*\mathrm{ts}}\left[\frac{1}{(1-m\sigma\lambda)(1+m\beta\lambda)}\right]^{1/2}, \tag{6}$$

where $u_{*\mathrm{tr}}$ is the threshold shear velocity of the rough surface, $u_{*\mathrm{ts}}$ is the threshold shear velocity for bare soil, m is an empirical factor, σ is the basal area index (rock basal area/ rock frontal area), λ is the roughness density, and β is the ratio of element drag to surface drag. In this study, data on rock size and distribution were collected

by ground surveys to calculate λ and σ. Measurements were made for the cover and dimensions of the rocks along 100-m transects, randomly allocated in the middle and eastern parts of the study area, where basalt rocks were scattered across the surface with different cover percentages. Results from rock measurements were used to calculate (λ) as follows:

$$\lambda = \frac{nbh}{s}, \tag{7}$$

where n represents the number of rocks, b is the width of the rock (m), h is the rock height (m), and S is the area (m^2) over which the rocks were distributed. The basal area was divided by the frontal area of the rock to calculate σ. The model was applied at a spatial resolution of 1.0 km. Each modelled cell was subsequently parsed into homogeneous sections based on LULC type, soil texture, and rock cover. For each time step, q was calculated for the proportion of bare soil within LULC, providing that $u_* > u_{*\mathrm{tr}}$. The q calculations for all subsections within the cell were then summed to produce q_{tot} associated with the wind speed for that time step of the modelled cell. The values of $u_{*\mathrm{ts}}$ and their own flux ratios were assigned for the different soil textures, based on values reported by Gillette (1980) and Gillete and Passi (1988).

The WE_DUST_EM also requires the wind field data, which was generated using the California Meteorological model (CALMET), the meteorological component of the California Puff model (CALPUFF). This model produced an hourly wind field grid after processing weather data and combining them with data related to surface cover. The CALMET system uses input meteorological data from both surface and upper air stations. The surface weather station data were hourly, while the upper air weather station data were collected twice a day; at hour 00.00 and at hour 12.00. Elevation data (DEM) and LULC were also entered to the model to calculate the wind speed at 10 m from the hourly data for each model grid cell. The output from CALMET was then used to calculate the value of u_* (shear velocity) for each cell from the following equation:

$$u_* = ku_z/\log(z/z_0), \tag{8}$$

where u_z is the average wind speed (m s^{-1}) at height z (m), k is von Karman's constant (0.4), and z_0 is the surface roughness. The values of z_0 were assigned in based on the LULC class.

WE_DUST_EM was run for the data from April to October for 10 years that covered the period 2001–2010. Histograms of wind speed data from two meteorological stations (Irbid and Mafraq) were generated to assess the frequency of occurrence and typify the study areas wind regime. Based on these histograms, wind speed was classified into three classes: low (<5 m s^{-1}); medium (5–10.9 m s^{-1}); and high (>10.9 m s^{-1}). The maps for soil erosion by wind were then generated for these three wind speed classes. An example is shown in figure 4 for the high-speed (low frequency) and the medium-speed (high frequency) wind events.

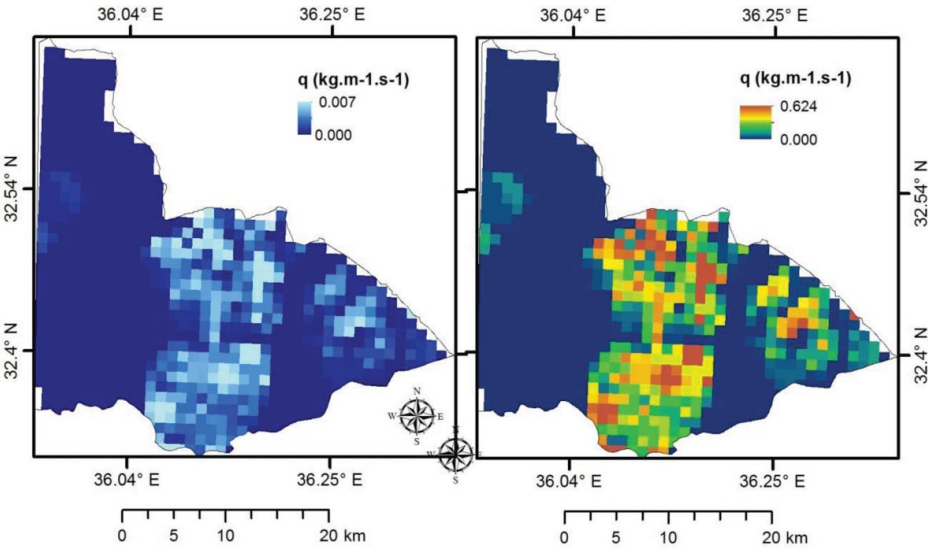

Figure 4. The modelled spatial distribution of horizontal flux representing the lower frequency (1%) high-wind speed events (left) and the dominant high-frequency (59%) medium-wind speed events (right).

2.4. *Modelling of drought*

A remotely sensed evapotranspiration water stress indicator (EWSI) was used for drought monitoring. The indicator is defined as follows (Suleiman & Al-Bakri 2011):

$$\mathrm{EWSI} = 1 - \frac{\mathrm{ET}a}{\mathrm{ET}c}, \tag{9}$$

where ETa is the actual daily evapotranspiration and ETc is the crop daily evapotranspiration. The EWSI values near 0 means that the ETa is close to the ETc implying no water stress within the modelled pixel. The EWSI value near 1 means that the actual evapotranspiration is very small compared to the ETc, indicating severe water stress for that pixel.

Calculation of ETc was carried out by multiplying the reference evapotranspiration (ETo), calculated with FAO-56 Penman–Monteith method (Allen et al. 1998), by the crop coefficient (Kc) map. This procedure was carried out by adding the values of Kc, recommended by Allen et al. (1998), as a new attribute to the LULC map to convert ETo to ETc. Modifications for these values were made to rainfed fields and rangelands by multiplying the Kc with the water stress coefficient (Ks), as described by Suleiman et al. (2008). Daily weather data to calculate ETo were obtained from the Jordan Meteorological Department.

The analytical land-atmosphere radiometer model (ALARM) was used to calculate ETa. The model, proposed by Suleiman and Crago (2002), was tested and calibrated in Jordan (Suleiman et al. 2008) to provide ETa estimates in the different ecological zones in the country, including the study area. The model computes ETa through the linkage between the evaporative heat fluxes (E) and land energy budget

equation (e.g. Brutsaert 1982) as follows:

$$E = (R_n - G)(1 - \Delta_T), \tag{10}$$

where R_n is the net incoming radiation (W m^{-2}), G is the heat flux into the ground (W m^{-2}), and Δ_T is the dimensionless temperature. ALARM was developed to convert satellite radiometric surface temperature to an aerodynamic surface temperature (Ti) at any view by correcting for the vegetation temperature profile and considering leaf area index (LAI), canopy height, fractional cover, leaf angle distribution, and sensor zenith view angle. In this model, Δ_T is calculated as follows (Suleiman & Al-Bakri 2011):

$$\Delta_T = \frac{Ti - T_a}{T_{\max} - T_a}, \tag{11}$$

where T_a and $T_{\max}$ are the average and the maximum air temperatures (°C), respectively. ALARM was run using remotely sensed data from the Moderate Resolution Imaging Spectroradiometer (MODIS). The data included images of the eight-day LAI, the 16-day albedo, and daily radiometric surface temperature at a resolution of 1 km. The images, downloaded from the MODIS data gateway (http://reverb.echo.nasa.gov/reverb/), were incorporated within ALARM to calculate the parameters for equation (10) and to derive ETa as described by Suleiman et al. (2008).

The work on drought mapping focused on identifying areas with obvious changes in EWSI for each year during 2001–2010 for four-month periods separately. These included January (mid-winter), March (spring), May (early summer), and November (late autumn). The EWSI difference maps were then prepared by subtracting the EWSI map for each of the four-month periods during 2002–2010 with the EWSI map for the same period in 2001. The values of EWSI in the year 2001 were taken as a reference. In terms of rainfall amount, year 2001 was dry and rainfall was about 50%–65% of the average. In Irbid station, for example, the 2001 rainfall was 278 mm, while the 2001–2010 average was 450 mm. Therefore, the aim of comparison was to detect the count of years when EWSI was improving, i.e. getting lower than in 2001. The zero count would imply that the EWSI did not decrease in any year between 2002 and 2010, while positive counts corresponded to the number of years when EWSI was decreasing, implying more water stress during that particular period of the year. A map representing the average EWSI difference for 2002–2010 compared with 2001 for the different periods of the season was prepared for the desertification model.

2.5. *Incorporating maps for mapping desertification risk*

Maps of soil erosion and drought were incorporated in GIS to generate the desertification risk map. Each of the three maps was reclassified into four classes: slight, moderate, severe, and very severe. The classes for water erosion were based on ranges reported in Mediterranean environments similar to our study area (Andersson 2010). The wind erosion maps for horizontal flux were reclassified into four levels (figure 5) for the medium-speed high-frequency wind events. Since wind erosion modelling with WE_DUST_EM was not carried out in Jordan before this study, classification

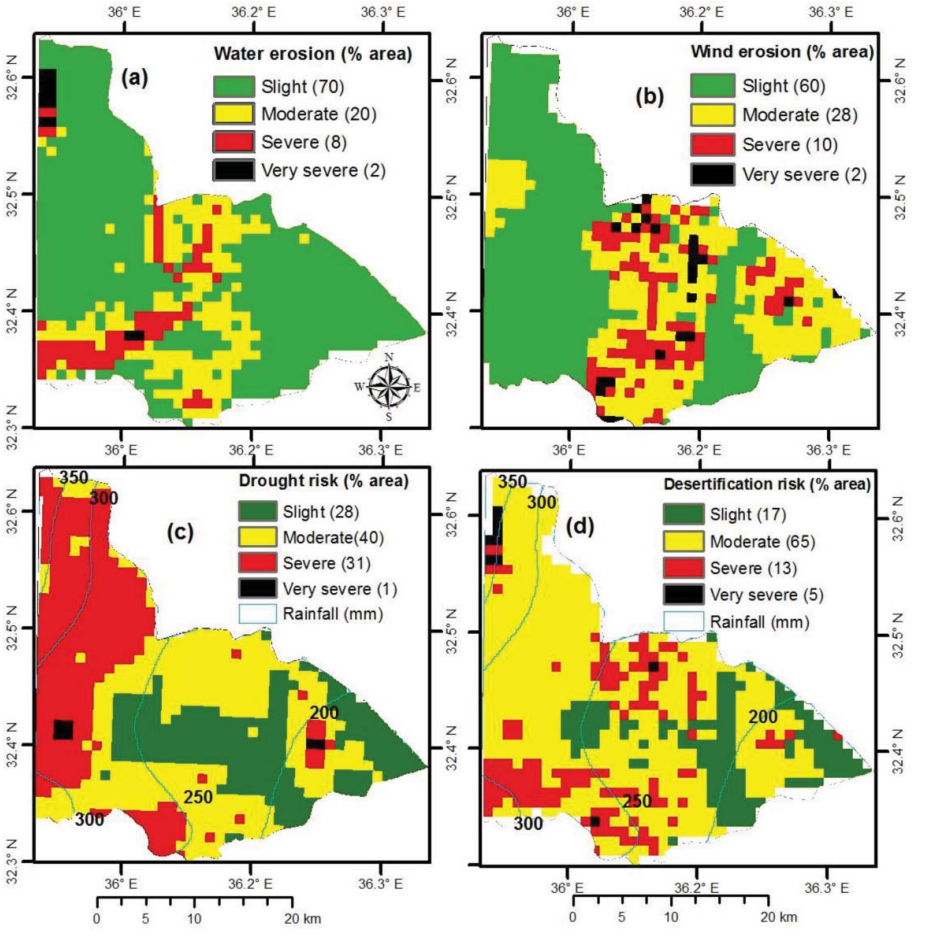

Figure 5. Maps of desertification risk-based water erosion (a), wind erosion (b), EWSI (c), and the sum of soil erosion and EWSI (d).

of the maps was based on the values of the mean and standard deviation of q for the horizontal flux for medium-wind speed, as the histogram exhibited a normal distribution pattern. The EWSI maps were reclassified based on the number of years when EWSI was worse than the baseline year of calculation, i.e. year 2001. Based on the count of EWSI decrease during 2002–2010, the EWSI maps were classified into four classes based on counts of decrease: slight (>7), moderate (5–6), severe (3–4), and very severe (0–2). Following the stage of reclassification, the sum overlay function was used to merge the three maps into a map representing desertification risk in the study area.

2.6. *Analysis of maps*

An exploratory regression analysis was carried out for the maps of soil erosion by water to identify the most important factor contributing to this process in the study

area. The same statistical analysis was carried out for the GIS layers for the factors that were contributing to wind erosion. For the map of EWSI difference, an intersection with LULC was carried out to assess the spatial distribution of drought in relation to land use. Within the GIS, the exploratory regression analysis evaluates all possible combinations of the input layers of explanatory variables that best explain the dependent variable. While exploratory regression is similar to stepwise regression (found in many statistical software packages), rather than only looking for models with high adjusted R^2 (coefficient of determination) values, it also looks for models that meet all of the requirements and assumptions of the global ordinary least squares method (OLS). The OLS is the best known of all regression techniques as it provides a global model of the investigated variable or process to understand or predict by creating a single regression equation to represent that process (Griffith 1987; Burnham & Anderson 2002).

To apply the exploratory regression, the maps of the USLE factors were used as independent variables that could explain the final map of soil erosion by water, after converting all maps from raster into vector format. For the wind erosion map, the independent variables included the maps of soil content of sand, rock percentage, and the map of LULC. The variables included in the regression represent the soil properties that, with the addition of wind speed, could explain the spatial distribution of wind erosion. The statistical analysis included the Moran's I statistics that would indicate the tendency of each map toward clustering based on its Z-score and associated p-value. The results from OLS and exploratory regression also included the assessment of model significance (using Joint F and Wald Statistics), redundancy of variables (indicated by variance inflation factor, VIF), and the normality of the model residuals for each variable (using Jarque–Bera statistics (J–B)) (Burnham & Anderson 2002).

3. Results and Discussion

3.1. Soil erosion by water

Results from USLE showed that the expected soil loss by water was in the range of 0.1–28.0 ton ha^{-1} $year^{-1}$ with an average rate of 2.3 ton ha^{-1} $year^{-1}$. Analysis of the soil erosion map showed that 90% of the study area had an erosion rate of less than 5.0 ton ha^{-1} $year^{-1}$ (figure 5). About 8% of the study area had a relatively high rate of soil erosion that exceeded 10.1 ton ha^{-1} $year^{-1}$. Analysis of the spatial distribution of soil erosion showed that the map (figure 2) had a clustered pattern; as indicated by the significant Moran I index with a positive Z-score of 27.3 that exceeded the critical value (1.96; $p < 0.05$). The main variable which contributed to this pattern was LS (table 1), which explained about 68% of the variations in soil erosion, followed by C which explained about 17% of the variations in this pattern.

The histograms of residuals showed that none of the factors was normally distributed. The P and LS were more biased towards low values while the C and K factors were biased towards the high values. This could be attributed to the low vegetation cover of rainfed crops during rainy season and the sparse vegetation cover in the open rangelands, as indicated by Al-Bakri and Taylor (2003) and Al-Bakri et al. (2012). Therefore, the absence of protective vegetation cover and appropriate land management (P-factor) could enhance soil erosion in areas with steep slopes.

Table 1. Summary of exploratory regression analysis and OLS for the map of soil erosion by water.

Exploratory regression				OLS for regression***			
Adjusted R^2	Variable	VIF*	P for J-B **	Variable	Coefficient	Standard error	VIF*
0.68	LS	1.00	<0.05	Intercept	−9.61	1.60	–
0.17	*C*	1.00	<0.05	*C*	4.28	0.43	1.30
0.09	*R*	1.00	<0.05	*K*	49.13	7.72	1.72
0.73	LS, *C*	1.06	<0.05	LS	0.95	0.03	1.23
0.69	LS, *K*	1.04	<0.05	*P*	4.01	2.47	1.14
0.68	LS, *P*	1.04	<0.05	*R*	0.04	0.01	1.65
0.73	LS, *K*, *C*	1.20	<0.05				
0.73	LS, *R*, *C*	1.20	<0.05				
0.75	*C*, *K*, LS, *R*	1.67	<0.05				
0.75	All	1.72	<0.05				

* Large VIF (>7.5) indicates redundancy among the explanatory variables.
** Values < 0.1 indicating that residuals are not normally distributed.
*** Statistically significant ($p < 0.05$).

Levels of soil erosion by water were compared with findings from previous research on soil erosion in Jordan (Farhan & Al-Bakri 2012) and in the Mediterranean region (Martínez-Fernández 2004; Andersson 2010). Slight differences between the results of this study and results obtained by Farhan and Al-Bakri (2012) were observed. These could be attributed to the spatial resolution of the model, which was 30 m for the latter, although the mean soil loss from both studies was pretty close (2.3 and 2.1 ton ha^{-1} $year^{-1}$ for the 1 km and the 30 m, respectively). The average rate of soil erosion in the study area was within the range (0.5–3.0 ton ha^{-1} $year^{-1}$) reported in other Mediterranean areas (Martínez-Fernández 2004; Andersson 2010). The results of this study agreed with USLE results for a similar Mediterranean area in Tunisia (Andersson 2010) where the maximum erosion rate was 24.5 ton ha^{-1} $year^{-1}$, pretty close to the maximum obtained from this study (28.0 ton ha^{-1} $year^{-1}$). The relatively high levels of soil erosion emphasize the need for implementing soil conservation and erosion control measures, such as contour plowing, terracing, and stonewall construction on farmer's fields to reduce soil erosion and to conserve the productivity of agricultural lands. The failure to convince farmers to adopt these land management practices has accelerated soil erosion and desertification in the rainfed agricultural areas of Jordan (Al-Alawi 2008; Khresat et al. 2008).

3.2. *Soil erosion by wind*

The first output from the wind erosion model was the analysis and classification of the main classes of wind speed using CALMET (table 2). Output from this analysis showed that wind speed exhibited a normal distribution and occurred most frequently (59%) at 5–10 m s^{-1} (classified as medium wind speed). Overall, the days with low wind speeds were more numerous than the days with the medium and high wind speeds and the threshold shear velocity was not met. When the threshold shear

Table 2. Frequency for each class of hourly wind speed from May to October.

Class	Speed ($m\ s^{-1}$)	Frequency (%)	Frequency (%) used in the model	Total days of occurrence	Month of occurrence and its proportion (%)
Calm wind (no wind erosion occurs)	0.0	18.57	17.2	N/A	N/A
	0.1	8.58			
Low wind speed	2.5	13.4	13.4	83	June (9.6), July (45.8), August (18.1), and October (26.5)
Medium wind speed	5.0	44.03	58.8	76	May (5.3), June (9.2), July (60.5), August (18.4), and October (6.6)
	7.5	12.72			
	10.0	2.05			
High wind speed	12.5	0.35	0.7	10	May (30), June (20), and August (50)
	15.0	0.11			
	17.5	0.13			
	20.0	0.03			
	22.5	0.08			
	25.0	<0.01			

velocity was exceeded in the medium and high wind speed events and erosion was expected to occur, the cumulative horizontal flux was greater for the medium wind speed class than for the high wind speed (figure 4), due to the higher frequency of the medium wind speed class.

The map of long-term wind erosion (figure 5) showed that high levels of soil erosion occurred most frequently in the central and the north-eastern parts of the study area. In terms of spatial pattern, statistical analysis showed that soil erosion had a clustered pattern, as indicated by the significant Moran *I* index (value of 0.63) with a positive *Z*-score of 27.7 ($p < 0.01$). The main factor that was contributing to soil erosion was the wind speed, which reached slightly over 20 $m\ s^{-1}$ on several dates during late spring and summer. Exposed bare soil and soil texture also contributed to the high levels of soil erosion by wind. Results of exploratory regression and OLS (table 3) showed that the factors of rock cover, soil content of sand, elevation, and LULC explained 25% of the variations in wind erosion, as indicated by the R^2 value which reached 0.25. Therefore, results from this study indicate that wind speed was the main factor contributing to the problem of soil erosion outside the rainy season. These results are also in agreement with the findings of He et al. (2011), who found that climatic factors were the main contributors to wind erosion. Comparing results of WE_DUST_EM in the study area with the levels of erosion reported in other arid environments (as summarized by Brown (2007)) showed high levels of soil erosion by wind. This finding could be attributed to the poor conditions of the soil and the unsupervised land management practices of overgrazing, which in turn accelerated this land degradation process.

Table 3. Summary of exploratory regression analysis and OLS for the map of soil erosion by wind.

Exploratory regression				OLS for regression with all variables***			
Adjusted R^2	Variable	VIF*	P for J-B **	Variable	Coefficient	Standard error	VIF*
0.16	Rock (RK)	1.00	<0.05	Intercept	−0.33758	0.03508	–
0.07	Elevation (EL)	1.00	<0.05	EL	0.00028	0.00004	1.03
0.07	Sand (SA)	1.00	<0.05	LULC	0.00192	0.00059	1.02
0.21	EL, RK	1.02	<0.05	RK	0.00393	0.00041	1.09
0.25	RK, SA, LUL C	1.09	<0.05	SA	0.00665	0.00155	1.08
0.25	All	1.13	<0.05				

* Large VIF (>7.5) indicates redundancy among the explanatory variables.
** Values <0.1 indicating that residuals are not normally distributed.
*** Statistically significant ($p < 0.05$).

3.3. *Extent of drought*

Results showed that EWSI was decreasing during 2002−2010 when compared with the values of 2001. The pattern of EWSI change over time was different across the region, indicating different levels of water stress in the study area. Generally, the area of highest water stress was located in the relatively high rainfall zone in the west (figure 5). This could be attributed to the higher crop water requirements for the rainfed crops of wheat and olives in this zone when compared with barley in the low rainfall zone.

Results showed that 31% of the area was suffering from severe drought during 2002−2010 when compared with 2001. Since water stress would vary with vegetation and land management, the EWSI difference maps were intersected with the LULC map.

Results of this analysis showed that agricultural lands and open rangelands were the main areas suffering from water stress (table 4). In May, the extent of stress was larger for rainfed area than for rangelands, while the opposite was observed in November. This would indicate the low levels of soil moisture in these periods of the year. The stressed areas in May and November were 179 and 189 km^2, respectively.

Table 4. Area of each land use/land cover type under water stress.

	Area (km^2) with water stress		
Land use/land cover	March	May	November
Mixed rainfed areas	13.5	92.8	31.0
Open rangeland	2.8	48.3	105.8
Irrigated areas	0.0	19.8	31.2
Protected areas	0.0	0.0	0.1
Others	0.1	18.0	20.7
Total	16.3	178.9	188.7

These figures correspond to 18 and 19% of the total area for each month, respectively.

An important output from this comparison was also the impact of management on desertification, as indicated by EWSI. Analysis of maps showed that the stressed area of open rangeland reached 106 km^2 (11% of the total area), while nearly no water stress was taking place inside the protected areas. These figures imply that there was inappropriate management of rangelands in the study area. These results complement the soil erosion mapping as they detected an important aspect of desertification (drought) in the high rainfall zones in the study area. Also, they suggest that land use shifts from rainfed trees and wheat into rainfed barley and/or open rangeland could be considered as an important indicator for desertification as they reflect farmers' adaptation to successive droughts.

3.4. *Desertification risk*

Most of the study area had moderate desertification risk, but 18% of the study area had severe to very severe desertification risk. Considering soil erosion alone in desertification assessment resulted in classifying most of the western parts of the study area as slight risk. This result can be attributed to the flat topography and the relatively good vegetation cover. When EWSI was considered in the desertification model, spatial patterns of desertification risk changed and showed that drought was an important natural hazard that is also contributing to desertification.

In terms of the spatial distribution of desertification, the final map of desertification risk (figure 5) showed that severe risk was associated with the 250–300 mm rainfall isohyets, while most of the area with 200 mm rainfall or less was characterized by slight to moderate risk. The reason behind this counterintuitive finding could be that most of this area was irrigated and therefore did not suffer from water stress. Irrigation, however, should not be taken as a sustainable solution to alleviate the problem of desertification. In Jordan, overpumping of groundwater to irrigate agricultural crops was found to be an adverse factor that caused salinization of soil and accelerated the problem of desertification in the country (MoEnv 2006, Al-Bakri et al. 2012).

In terms of wind erosion, results showed that the study area is at a moderate desertification risk. This risk increases due to the impact of EWSI on the desertification risk model; this highlights the importance of combining the different land degradation processes within the desertification model. Under the trends of increased temperature and decreased rainfall amounts in the region (Al-Bakri et al. 2013), drought would trigger the problem of desertification in the country and might result in shifts in cropping patterns or in increased abandonment of agricultural lands.

4. Conclusions

Results showed that the WE_DUST_EM and USLE models could be combined for mapping the spatial distribution of soil erosion in the study area. The EWSI maps added important information on the extent of land degradation resulting from drought in the relatively high rainfall parts of the study area. As most of the parameters for these models were obtained from remotely sensed data, the study emphasized the important roles of these emerging techniques in mapping natural and

human-induced hazards and risks. Therefore, adoption of the models tested in this study is recommended to extend desertification risk mapping for other parts of Jordan. Application of these models for similar Mediterranean environments is also possible, as most of the inputs for the models are available from remotely sensed data and geospatial databases. Future improvements to this approach may include the application of these GIS-based models at finer spatial resolutions and the inclusion of other remotely sensed parameters in the models. In terms of desertification risk, the models deployed in this study identified climate and land mismanagement as the main drivers of soil erosion and desertification in the Yarmouk basin. Therefore, prevention/mitigation measures should be prioritized for areas with severe desertification risks.

Acknowledgements

The authors acknowledge Azzam Ananbeh, Tarek Kandakji, Sari Shawash, and Ibrahim Farhan from the University of Jordan for their efforts in field surveys and preparation of data.

Funding

This work was supported by the NATO's Science for Peace Program, project SfP-983368 "Assessment and monitoring of desertification in Jordan using remote sensing and bioindicators".

References

Al-Alawi M. 2008. Desertification in Jordan. In: Liotta PH, Mouat DA, Kepner WG, Lancaster J, editors. Environmental change and human security: recognizing and acting on hazard impacts. NATO Science for Peace and Security Series C: Environmental Security. Springer. doi:10.1007/978-1-4020-8551-2_5

Al-Bakri J, Saoub H, Nickling W, Suleiman A, Salahat M, Khresat S, Kandakji T. 2012. Remote sensing indices for monitoring land degradation in a semiarid to arid basin in Jordan. Proceedings of SPIE 8538, Earth Resources and Environmental Remote Sensing/GIS Applications III, 853810; 2012 September 24; 2012 October 25. Edinburgh, UK. doi:10.1117/12.974333

Al-Bakri JT, Salahat M, Suleiman A, Suifan M, Hamdan MR, Khresat S, Kandakji T. 2013. Impact of climate and land use changes on water and food security in Jordan: implications for transcending "the tragedy of the commons". Sustainability. 5:724–748.

Al-Bakri JT, Taylor JC. 2003. Application of NOAA-AVHRR for monitoring vegetation conditions and biomass in Jordan. J Arid Environ. 54:579–593.

Al-Hadidi L. 1996. Evaluation of desertification risk in Jordan using some climatic factors [Unpublished MSc Thesis]. Amman: The University of Jordan.

Allen RG, Pereira LA, Raes D, Smith M. 1998. "Crop evapotranspiration". *FAO Irrigation and Drainage Paper* 56. Rome: FAO; p. 293.

Al-Zitawi F. 2006. Using RUSLE in prediction of soil loss for selected sites in north and northwest of Jordan [Unpublished MSc Thesis]. Irbid: University of Science and Technology.

Andersson L. 2010. Soil loss estimation based on the USLE/GIS approach through small catchments – a minor field study in Tunisia [MSc Thesis]. Lund: Lund University.

Brown LJ. 2007. Wind erosion in sparsely vegetated rangelands [PhD dissertation]. Guelph: University of Guelph.

Brutsaert W. 1982. Evaporation into the atmosphere: theory, history, and applications. Dordrecht, Holland: D. Reidel Publishing Company; p. 299.

Burnham KP, Anderson DR. 2002. Model selection and multimodel inference: a practical information-theoretic approach. 2nd ed. New York (NY): Springer.

Dregne HE. 2002. Land degradation in the drylands. Arid Land Res Manag. 16:99–132.

El-Taif NI, Gharaibeh MA, Al-Zaitawi F, Alhamad MN. 2010. Approximation of rainfall erosivity factors in north Jordan. J Pedosphere. 20:711–717.

Essa S. 2004. GIS modeling of land degradation in northern Jordan using Landsat imagery. In: Altan MO, editor. Geo-imagery bridging continents, the XXth ISPRS Congress; 2004 July 12–23; Vol XXXV, Part B4. Istanbul, Turkey: ISPRS; p. 505–510.

Farhan IA, Al-Bakri JT. 2012. Use of GIS and remote sensing to assess soil erosion in arid to semiarid basin in Jordan. In: Aksoy H, Mahe G, Özen B, Touaibia B, Akay O, Köroğlu A, editors. Proceedings of the International Conference on Sediment transport modelling in hydrological watersheds and rivers; 2012 November 14–16. Istanbul, Turkey: MEDFRIEND Publishing; p. 145–152.

Fistikogli O, Harmancioglu NB. 2002. Integration of GIS with USLE in assessment of soil erosion. J Water Resour Manag. 16:447–467.

[FAO/UNEP] Food and Agriculture Organization/United Nations Environment Programme. 1984. Provisional methodology for assessment and mapping of desertification, Rome: FAO.

Gillette DA. 1980. Major contributions of natural primary continental aerosols: source mechanisms. Ann N Y Acad Sci. 338:348–358.

Gillete DA, Passi R. 1988. Modeling dust emission caused by wind erosion. J Geophysical Res. 93:14234–14242.

Griffith D. 1987. Spatial autocorrelation: a primer. Resource Publications in Geography, Washington (DC): Association of American Geographers.

He Q, Yang XH, Mamtimin A, Tang S. 2011. Impact factors of soil wind erosion in the center of Taklimakan desert. J Arid Land. 3:9–14.

Kepner WG, Rubio JL, Mouat DA, Pedrazzini F. 2006. Desertification in the mediterranean region: a security issue. Vol. 3, NATO Security through Science Series. Netherlands: Springer. doi:10.1007/1-4020-3760-0

Khosrokhania M, Pradhan B. 2013. Spatio-temporal assessment of soil erosion at Kuala Lumpur metropolitan city using remote sensing data and GIS. Geomatics Nat Hazard Risk. 5:252–270.

Khresat S, Al-Bakri J, Tahhan R. 2008. Impacts of land use change on soil properties in the Mediterranean region of northwestern Jordan. Land Degradation Dev. 19:397–407.

Martínez-Fernández J. 2004. Which is the real desertification problem in Spain? A critical perspective. In: Enne G, Peter D, Zanolla C, Zucca C, editors. The MEDRAP concerted action to support the northern Mediterranean action programme to combat desertification. Sassari: University of Sassari; p. 616–628.

Millán MM, Estrela MJ, Sanz MJ, Mantilla E, Martín M, Pastor F, Salvador R, Vallejo R, Alonso L, Gangoiti G, et al. 2005. Climatic feedbacks and desertification: the Mediterranean model. J Clim. 18:684–701.

[MOA] Ministry of Agriculture, Jordan. 1994. The soils of Jordan: semi-detailed level (1:50 000). The National Soil Map and Land Use Project. Amman: Ministry of Agriculture.

[MoEnv] Ministry of Environment, Jordan. 2006. National action plan and strategy to combat desertification; Deposit no. 2004/1/70; Amman: Ministry of Environment.

Mitasova H, Hofierka J, Zlocha M, Iverson RL. 1996. Modeling topographic potential for erosion and deposition using GIS. Int J Geographical Inf Sci. 10:629–641.

Namikas S, Sherman D. 1997. Predicting aeolian sand transport: revisiting the White model. Earth Surf Process Landforms. 22:601–604.

Raupach MR, Gillette DA, Leys JF. 1993. The effect of roughness elements on wind erosion threshold. J Geophysical Res. 98:3023–3029.

Santini M, Caccamo G, Laurenti A, Noce S, Valentini R. 2010. A multi-component GIS framework for desertification risk assessment by an integrated index. App Geogr. 30:394–415.

Saïdi S, Gintzburger G. 2013. A spatial desertification indicator for Mediterranean arid rangelands: a case study in Algeria. Rangeland J. 35:47–62.

Sarre RD. 1988. An evaluation of aeolian sand transport equations using intertidal zone measurements, Saunton Sands, England. Sedimentology. 35:671–679.

Suleiman A, Al-Bakri J. 2011. Estimating actual evapotranspiration using ALARM and the dimensionless temperature. In: Labedzki L, editor. Evapotranspiration. Croatia: InTech Publisher; p.163–194. http://www.intechopen.com/articles/show/title/estimating-actual-evapotranspiration-using-alarm-and-the-dimensionless-temperature.

Suleiman A, Al-Bakri JT, Duqqah M, Crago R. 2008. Intercomparison of evapotranspiration estimates at the different ecological zones in Jordan. J Hydrometeorology. 9:903–919.

Suleiman AA, Crago RD. 2002. Analytical land atmosphere radiometer model. J App Meteorol. 41:177–187.

[UNCCD] United Nation Convention to Combat Desertification. 1994. United Nations Convention to Combat Desertification. General Assembly, UN. Available from: http://www.unccd.int/

[UNCCD] United Nation Convention to Combat Desertification. 2009. The UNCCD 1st Scientific Conference: Synthesis and recommendations and COPs-CST Ninth session; 2009 September 22–25; Buenos Aires Bonn, Germany: UNCCD.

[UNEP] United Nations Environment Programme. 1992. United Nations Conference on Environment & Development. Agenda 21, Chapter 12, Adopted at the Rio Conference June, 1992. New York (NY): United Nations.

Wischmeier WH, Smith DD. 1978. Predicting rainfall erosion losses: a guide to conservation planning. agriculture handbook. Washington (DC): USDA.

Zhai L, Feng Q. 2009. Spatial and temporal pattern of precipitation and drought in Gansu Province, northwest China. Nat Hazard. 49:1–24.